Materials Characterization 171 (2021) 110808

Contents lists available at ScienceDirect

Materials Characterization

journal homepage: www.elsevier.com/locate/matchar

An automated procedure built on MTEX for reconstructing deformation twin hierarchies from electron backscattered diffraction datasets of heavily twinned microstructures

Daniel J. Savage [a,b], Rodney J. McCabe [b], Marko Knezevic [a,*]

[a] Department of Mechanical Engineering, University of New Hampshire, Durham, NH 03824, USA
[b] Materials Science and Technology Division, Los Alamos National Laboratory, Los Alamos, NM 87545, USA

ARTICLE INFO

Keywords:
Microstructures
Twinning
Titanium
EBSD
MTEX

ABSTRACT

This paper presents a set of algorithms built on the MTEX and MATLAB graph toolboxes for automatic reconstruction of deformation twin hierarchies from Electron Backscatter Diffraction (EBSD) datasets with a focus on developing methods for heavily twinned microstructures (twin fractions >0.5). The algorithms address key issues arising at large strains, mainly: missing twin relationships, grouping of heavily deformed grain fragments into families of similar orientation originating from a single initial grain, identification of parent fragments for large twin volume fractions, and classification of families having twin relationships with multiple families. To facilitate the development of these algorithms, large-grained ultra-high purity α-Ti deformed in compression along two directions is investigated. Graphs are utilized to handle non-local geometric merging and to represent relationships throughout the reconstruction process. When determining if a grain fragment is from the undeformed microstructure, the combined metrics of the fragment's orientation volume fraction in the initial texture and the directed graph centrality measure of out-closeness (the number of nodes reached in a graph from a given node) are essential. To address automation in reconstructing the sequence of twinning and relating fragments originating from a single grain in the initial microstructure, the twin family tree is formulated as a minimum spanning tree emanating from the initial grain family. A scheme constructing the distances associated with twin relationship comprising the spanning tree is developed, and a novel quasi-directional Prim spanning tree algorithm is used to determine the twin family tree. The procedure is demonstrated to significantly improve the level of automation in reconstructing twin hierarchies in heavily twinned microstructure compared to other methodologies in literature. The procedure can readily be applied to analyses of twinning in metals, as well as provide an approach for routinely extracting twin statistics at larger deformation levels than previously possible. Significantly, the procedure is demonstrated to be capable of identifying third generation twinning in α-Ti microstructures.

1. Introduction

Deformation twinning is a shear-based transformation that results in crystal reorientation and significantly influences the evolution of local and overall material properties of many important metals undergoing twinning [1–3]. One well-known twin phenomena is the orientation dependent anisotropic hardening introduced by twin lamella fragmenting slip domains and reorienting towards hard crystal orientations [4–8]. In addition to hardening, many studies show the formation of twins are correlated to flow localization and ultimately void/crack formation in the vicinity of their boundaries [9–15]. This correlation has been rationalized to arise due to substantial crystal reorientations and underlying shifts in active crystallographic slip modes within the twinned domain. Furthermore, collection of nucleation statistics such as in fatigue loading, is vital to building the understanding of fracture in hexagonal close-packed (HCP) materials [16]. Thus, measuring and classifying twinning is relevant for developing a working knowledge of fracture and the anisotropic response of materials.

Twinning plays an important role in developing Integrated Computational Materials Engineering (ICME) toolsets. Crystal plasticity

* Corresponding author at: University of New Hampshire, Department of Mechanical Engineering, 33 Academic Way, Kingsbury Hall, W119, Durham, NH 03824, USA.
E-mail address: marko.knezevic@unh.edu (M. Knezevic).

https://doi.org/10.1016/j.matchar.2020.110808
Received 3 September 2020; Received in revised form 17 November 2020; Accepted 24 November 2020
Available online 4 December 2020

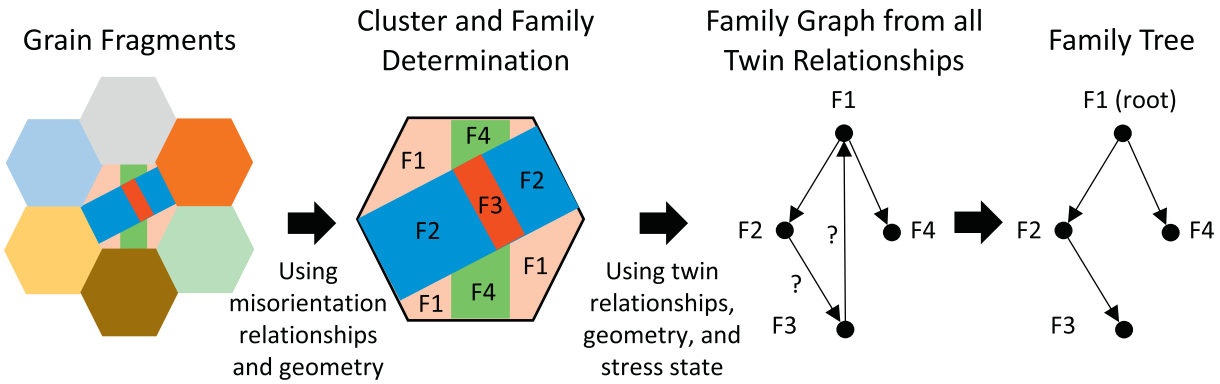

Fig. 1. Schematic of the tasks and challenges performed in twin codes (from left to right): identification of twin relationships and grouping of grain fragments (clusters), identification of fragments of the same orientation (families, F), and the determination of the representative family tree. Note that a cluster is the group of families comprising a single grain in the initial microstructure. Shown is an example of the family tree where the F1 family is the parent of families F2 and F4, and F3 is a second generation twin whose parent is F2. A circular twin relationship (e.g. F1, F2, F3, and F1) arises from the combination of twin crystallographic reorientations and a twin code must identify the correct twin hierarchy. The circular relationship causes no root (the family that is not a twin) to be evident based on the directions of twin relationships, and another criterion (presented in this work) is needed to determine the root automatically.

constitutive laws, for instance, enable ICME [17–25] by modeling strain path dependent deformation behavior of highly anisotropic metals through the evolution of slip, twin, and phase-induced texture evolution [26,27]. In HCP and lower symmetry metals such as orthorhombic metals [28–33], it is usually necessary to emulate the twinning process, reproducing the statistics of experimental data to capture the mechanical response during complex loading [27,34,35]. The emulation of the twinning process requires detailed knowledge of the twin types, twin fractions, twin nucleation criterion, and their role in hardening the material; and ICME relies on the ability to extract twin-based information.

Considering the importance of twinning in fracture and understanding the anisotropic response of materials, several automatic twin identification codes have been published over the past two decades [36–40]. Two fundamental tasks are addressed in each implementation (see Fig. 1 for a graphical explanation): 1) determination of twin relationships based on boundary or mean fragment misorientation, grouping grain fragments (local EBSD regions of similar orientation) that composed a single grain in the initial microstructure (cluster), and grouping fragments in a cluster that have similar orientation (families); and 2) determination of the direction of the twin relationships (i.e. determining the pre-twinning (parent) and the twin (child) grain fragments) from which the family in the initial microstructure (root) is related to other families in a cluster (family tree). From these basic grouping and directional relationships, statistical analysis of twin activation, area fraction, number of lamella, twin thickness, and twin-twin junctions can be utilized to give a greater understanding of how deformation twinning evolves in materials [16,41–47].

Post-mortem, quantitative analysis of deformation twinning is challenging in highly deformed microstructures (strain >0.1) [48–51] due to the combination of reorientation by slip and twinning and the amount of microstructure fragmentation. In high-purity α-Ti, profusely twinned grains are observed with an abundance of primary tensile $\left\{10\bar{1}2\right\}\left\langle 10\bar{1}\bar{1}\right\rangle$ twins, secondary compression $\left\{11\bar{2}2\right\}\left\langle 11\bar{2}3\right\rangle$ twins, and even trace amounts of tertiary twins [52]. Statistically relevant analysis of higher ordering twinning has not been performed on α-Ti. Indeed, analysis of higher order twins using statistically relevant datasets is notably absent from current literature due to the challenges of automatic twin identification after high levels of deformation and twin hierarchies being analyzed using deterministic twin codes [36]. Examples of non-flexible twin code attributes include using only local misorientation relationships to identify twin relationships, handling circular relationship explicitly, assuming internal family misorientation can be appropriately grouped with a single tolerance, determining the root by area majority rule, and relying heavily on fragment geometry to determine the twin. To address fundamental issues regarding post-mortem analysis and slip, inverse modeling of the twinning process (e.g. through physically based crystal plasticity modeling) in addition to traditional twin identification approaches are needed. Key to this combined approach is a highly flexible framework that has the capability to assimilate all levels of microstructure and modeling information into a coherent interpretation of the microstructure evolution.

Volume fractions of twins in highly deformed microstructures have been determined using boundary length fractions and texture based methods. The boundary length fraction method is based on measuring the fraction of high-angle boundaries in the microstructure consistent with the twin misorientation relationship. The boundary fraction method is not an accurate measure of twin fraction even for first-generation twins [38]. Alternatively, twin fractions can be estimated based on the change in orientation distribution as the area fraction of material that has undergone a significant change in orientation. For instance, in HCP metals, tensile $\left\{10\bar{1}2\right\}\left\langle 10\bar{1}\bar{1}\right\rangle$ twins tend to flip grain orientations to align the **c**-axis with the compression direction, and the twin fraction is estimated from large EBSD scans or neutron diffraction bulk texture measurements based on the quantitative change in fraction of **c**-axes within some angle to the compression direction [17,53]. The texture method is reliable except when there are multiple types or generations of twins [54], or at high strains where slip results in significant grain reorientations of similar magnitude to twin misorientations. In general, twin statistics beyond volume fraction are not available from the texture method.

The objective of the present paper is the development of a robust framework for analyzing statistically relevant twinning datasets with large twin fractions at large strain. Relationships between two objects, such as the twinning relationship between grain fragments, can be represented by a *graph*(V,E) wherein each object is a node V, and each relationship between two objects is represented by an edge E. The graph methodology has been widely applied in EBSD analysis. Central to the MTEX approach for working with orientation maps are graph based methods for reconstruction, cleaning, and segmentation of EBSD datasets [55]. A graph-like approach has also been used in twin codes for relating directional twin relationships as a family tree [36], and a graph theory approach was completely embraced in the recent twin code METIS [37], wherein multiple graphs were used to reconstruct EBSD data points into grain fragments, to relate grain fragments into clusters, and using the cluster graph to represent the relationships between families. One especially important contribution of [37] was the identification of graphs as a means for visually interacting with and correcting

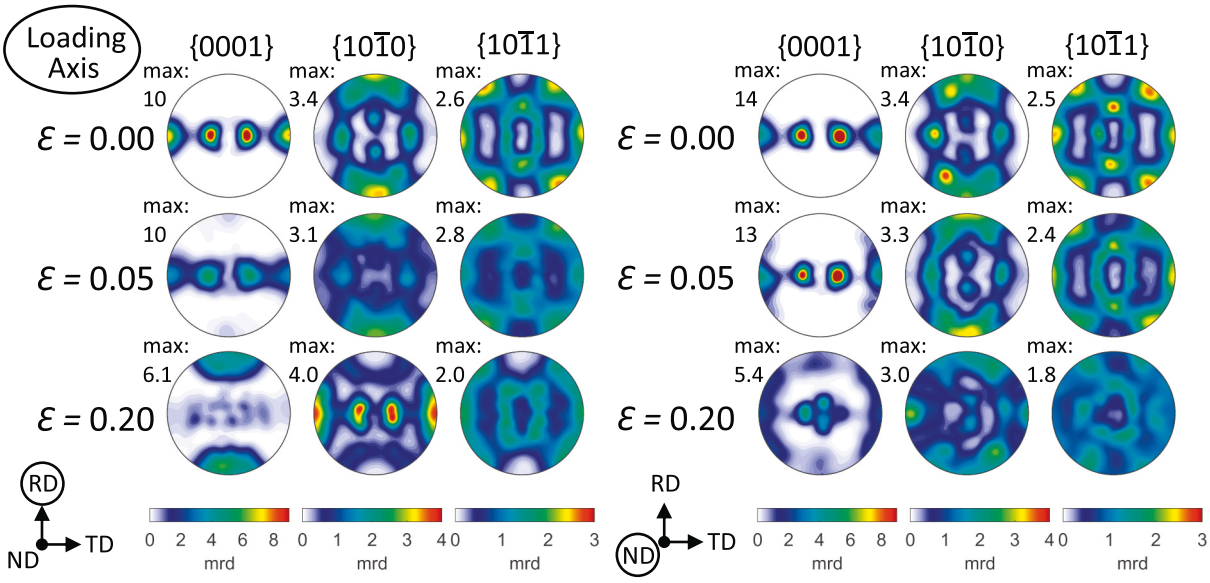

Fig. 2. Initial and deformed textures for loadings in RD (left) and ND (right). Textures were rotated to the sample frame for comparison.

data. This capability natively exists in MATLAB by combining the graph toolbox plotting with grain and EBSD plotting in MTEX, but has not been utilized in the literature on twinning thus far. Given the non-deterministic twinning behavior of materials [34,56,57] and inherent limitations in automatically identifying twins, a streamlined user interface is vital to cleaning large, statistically relevant datasets.

To the authors' knowledge, a twin code utilizing the MTEX framework has not been described in literature and would be helpful for the community, especially those using MTEX. Furthermore, twin codes in literature have largely been applied to low strain datasets (strain <0.1) due to lack of robust algorithms for twin identification and classification. In this work, we observe that grains with large twin volume fraction, many twin variants, higher order twinning, and internal misorientation, have not been sufficiently treated based on the descriptions of twin codes in literature. We leverage the flexibility and comprehensive texture analysis capabilities of MTEX and the MATLAB graph toolbox to address these shortcomings. The remainder of the text is organized as follows: in Section 2, we summarize the α-Ti datasets utilized in this work; in Section 3, the grain and family reconstruction algorithms are presented and manual interaction with graph data is described; in Section 4, the formation of the family tree for each cluster is given; and in Section 5, the segmentation produced by the twin code is discussed before summarizing findings in Section 6.

2. Experimental methods

A detailed description of the ultra-high purity (UHP) α-Ti material, sample fabrication, mechanical testing, electropolishing procedure, and data acquisition parameters is given in [58] and will only be briefly summarized here. A hot-rolled plate of UHP α-Ti was obtained from Fine Metals Corporation and had an elemental composition of 99.9993 at.% Ti with interstitial oxygen, carbon, and hydrogen at 219, 12.5, and 1 ppm, respectively. Blocks of materials were cut from the plate and heat-treated at 800 °C for 2 h in a sealed Lindberg/Blue tube furnace under an atmosphere of UHP Ar with a flow rate of 2 L/min. The heat treatment was followed by furnace cooling that resulted in large equiaxed grains with an average grain size of approximately 150μm (some sample to sample variation is report in Section 5, Table 3) and a strong initial texture (see Fig. 2). Cylindrical compression samples were fabricated to ASTM E9 standards using wire electrical discharge machining.

Compression testing was performed on a servo hydraulic INSTRON 1350 with a 100 kN load cell at a strain-rate of 10^{-3} s^{-1}. For this study, cylinders were loaded in compression along RD and ND directions. Compression testing was interrupted at true strains of 0.05 and 0.20 resulting in four deformed compression specimens. Samples were prepared for EBSD using the electropolishing procedure outlined in [58], and EBSD was performed on a TESCAN LYRA 3 GMU SEM at 20 kV with a HIKARI XP2 detector and a step size of 1.5μm for the initial microstructure and a maximum step size of 0.25μm for deformed microstructures. Data was collected in the plane perpendicular to the compression axis since twin statistics are not expected to be affected significantly by the section plane [45], and the scan was collected towards the end of the specimen and the axial position varied depending on the amount of material removed during EBSD preparation.

Table 1
Twin modes α, calculated axis angle pair for α-Ti, and twin reconstruction tolerances.

α	K_1	η_1	Angle [°]	Axis	β[°]	$\beta_{relaxed}$[°]	ϕ[°]
T_1	$\{10\bar{1}2\}$	$\langle\bar{1}011\rangle$	85.04	$\langle\bar{1}2\bar{1}0\rangle$	5	10	10
T_2	$\{11\bar{2}1\}$	$\langle\bar{1}\bar{1}26\rangle$	34.95	$\langle\bar{1}100\rangle$	2	10	10
C_1	$\{11\bar{2}2\}$	$\langle11\bar{2}\bar{3}\rangle$	64.40	$\langle\bar{1}100\rangle$	5	10	10

The lattice parameter used in calculating the axis angle pair is $c/a = 1.587$ and is taken from [63].

Initial and deformed textures for samples loaded along ND and TD were obtained via EBSD scans of the machined samples and are presented in Fig. 2. Approximately 1000 grains are used for the initial texture, and at least 400 clusters are used for the deformed texture (see Table 3 for detailed scan statistics). Insufficient grain statistics can lead to sharpening and fluctuations in texture components. However, the number of grains across the sample diameter is just 42 on average, and the textures are expected to be representative for the domain of the cross-section. A strong **c**-axis texture aligned towards TD at ~30° and 90° from ND is observed. Consequently, compressive loading along ND is favorable for both primary T_1 and C_1 twinning while RD is oriented for primary T_1 (see Table 1 for twin definitions). Small amounts of T_2 were observed and are included during the reconstruction.

The EBSD data used in the texture reconstruction in Fig. 2 was cleaned by performing confidence index (CI) standardization which assigns the maximum CI of a grain to all points in the grain. After the CI standardization data is removed with a CI less than 0.1 and grains with size less than 10 points are also removed. In all scans, less than 7% of

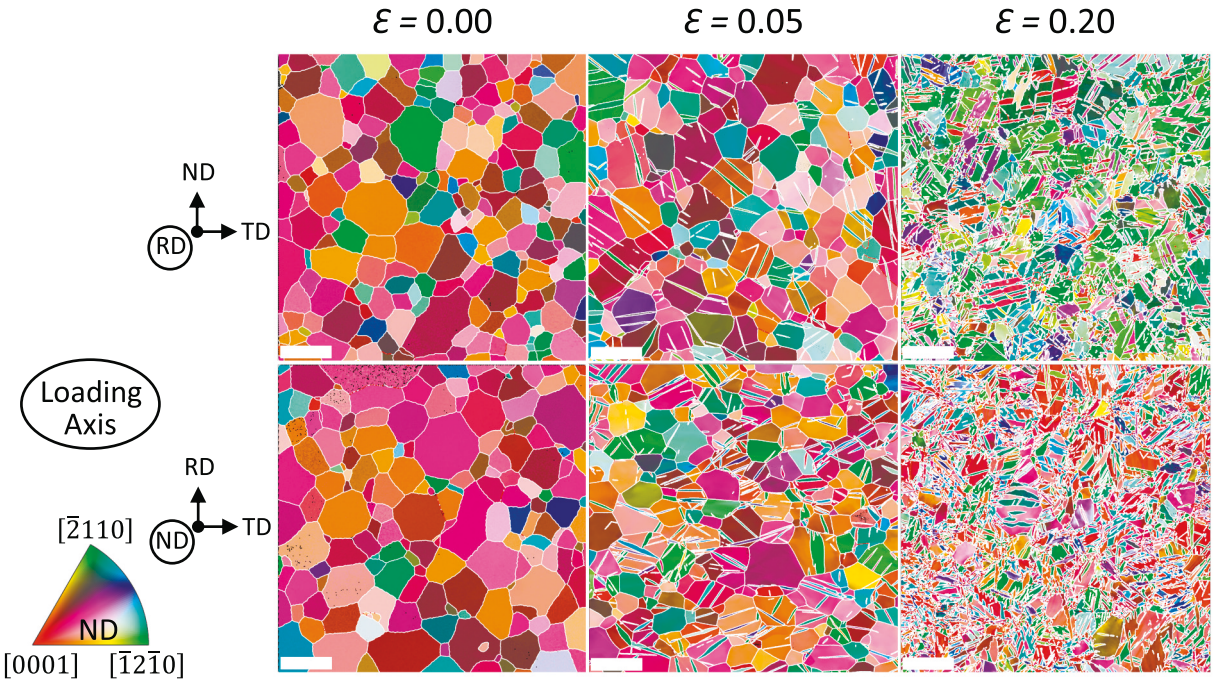

Fig. 3. Inverse pole figure (IPF) EBSD maps for initial microstructure and samples deformed in compression along RD and ND. The scans were collected in the plane of loading, and the EBSD spatial and crystal data was rotated in-plane based on texture to the designated frame before cropping to a view field of 1300 × 1300 μm. The white boundary overlay is for boundary misorientation greater than 5°. The scale bar is 200μm.

data points are removed by these thresholds. Grain fragments were reconstructed using the MTEX algorithm described in [55] and utilized a flood fill approach during grain reconstruction to treat points removed from EBSD data. In Fig. 3, the initial and deformed microstructures obtained with EBSD are presented with the reconstructed grain boundaries overlaid and black pixels representing removed EBSD pixels. Due to the strong texture, there are neighboring grains in the initial microstructure that have low angle boundaries. Furthermore, it is common in α-Ti for twins to chain together across grain boundaries, with only a small misorientation differentiating the twins. Adding a boundary due to under segmentation is not easily done, and biasing grain fragment reconstruction towards over segmentation is advantageous. To enable flexibility in partitioning low-angle boundaries in the construction of the cluster graph, grains were reconstructed with a $\theta_{frag} = 1^\circ$ misorientation tolerance for ND and a $\theta_{frag} = 2^\circ$ misorientation tolerance for RD. In the following sections, we use a number of misorientation tolerances and group them by applications:

- θ is utilized for EBSD fragment reconstruction
  - o θ_{frag} is the tolerance for grouping EBSD measurements into fragments
- β is utilized for cluster graph construction (grouping grain fragments that share a root into a cluster)
  - o β is the twin tolerance used to construct the starting cluster graph
  - o β_{frag} is the tolerance for merging grains of similar orientation
  - o β_{fam} is the tolerance for comparing mean family orientations during geometric merging
  - o $\beta_{relaxed}$ is used to identify twin relationships during geometric merging and manual modifications to the cluster graph
- α is utilized for family graph reconstruction (grouping fragments of similar orientation in a cluster)
  - o α_{fam} is the misorientation between a fragment and a mean family orientation which is used to determine if the fragment belongs to the family
  - o α_{frag} is the fragment to fragment misorientation tolerance for which fragments of two families will be merged
- ϕ is utilized for twin classification

3. Microstructure reconstruction

3.1. Definitions of twin misorientation relationships and equivalent Schmid factor

The twinning misorientation can be defined in terms of the twin composition plane K_1, twin shear direction η_1, the lattice parameters, twin type, and the crystal symmetry. MTEX is a comprehensive, versatile texture toolbox allowing several definitions of twin misorientations. Here a similar approach as in [36,59] considering the twin ($\mathbf{C}_{tw}$), crystal ($\mathbf{C}_c$), and sample frame ($\mathbf{C}_s$) is utilized to construct the twin misorientation, $\mathbf{M}_{tw}$, from which the axis-angle pairs and twin variants statistics are calculated using MTEX functions.

The twin misorientation, $\mathbf{R}_{tw}$, mapping the crystal frame to the twin frame is defined using the *map* function in MTEX such that $\mathbf{C}_{tw} = \mathbf{R}_{tw}\mathbf{C}_c$. To remain sufficiently general, three types of twins are discussed: (I) reflection about K_1, (II) a reorientation of 180° around η_1, and (III) a reorientation of 180° around K_1. Type I and III twins are equivalent for centrosymmetric crystals such as in α-Ti, but type III does not define a twin for non-centric crystals [59]. Thus, twins can be represented by either type I or type II twinning [60], and in the case that both type I and type II twinning are satisfied, a so called compound twin is formed. Choosing the shear direction and twin plane normal correspond to $\mathbf{e}_1^{tw}$ and $\mathbf{e}_3^{tw}$ in $\mathbf{C}_{tw}$, the rotations describing the twinning types can be taken as

$$\mathbf{T}^{I} = \begin{pmatrix} -1 & 0 & 0 \\ 0 & -1 & 0 \\ 0 & 0 & 1 \end{pmatrix}, \quad \mathbf{T}^{II} = \begin{pmatrix} 1 & 0 & 0 \\ 0 & -1 & 0 \\ 0 & 0 & -1 \end{pmatrix} \tag{1}$$

and the twin misorientation is given by

$$\mathbf{M}_{tw} = \mathbf{R}_{tw}^{T}\mathbf{T}\mathbf{R}_{tw} \tag{2}$$

In the case of sequential twinning where the primary boundary is missing (e.g. [17,61]), the misorientation in (2) can be multiplied by a

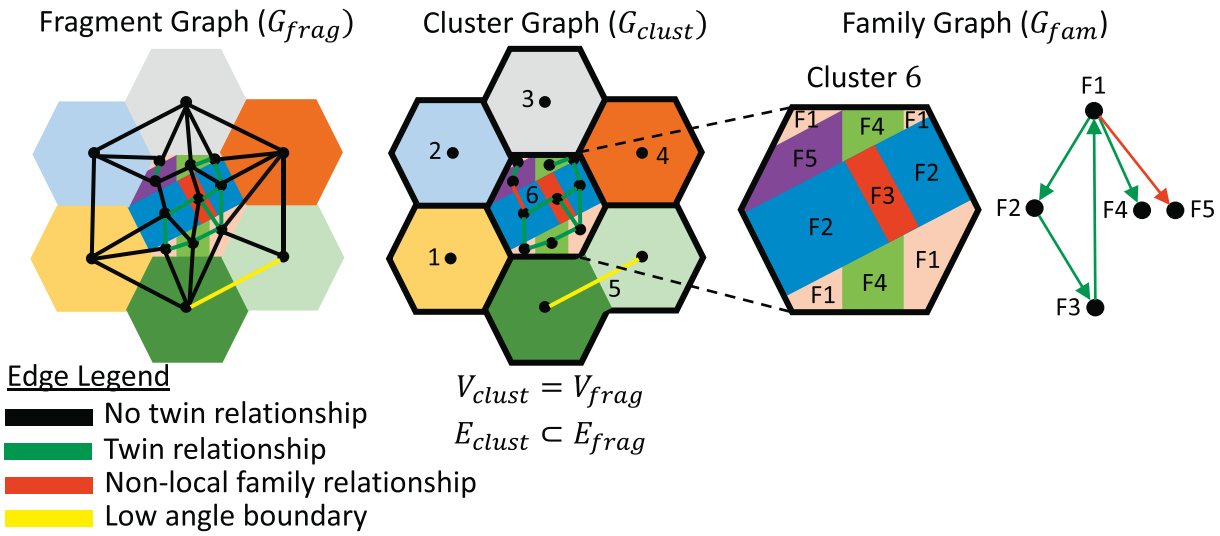

Fig. 4. Summary of the three main graphs used in this work and their relationships to each other. In the fragment graph (spanning multiple grains of the initial microstructure), each fragment is a node, and edges connect fragments that share boundaries. The cluster graph (spanning multiple clusters) has the same nodes as the fragment graph, and its edges are a subset of the fragment edges such that continuously connected regions are clusters. The family graph is defined per cluster with nodes representing a family and edges twin relationships. The family tree is a subset of the family graph. The red edge relation is included in the cluster due to identification that F1 is present in a neighboring cluster and a geometric condition (e.g. cluster size) is satisfied for the merging to occur. (For interpretation of the references to colour in this figure legend, the reader is referred to the web version of this article.)

second misorientation to specify the combined misorientation and build the relevant secondary twin mode variants. Twinning is directional and twin variants are defined by applying the collection of rotation operations to a twin variant. For instance, in α-Ti the six twin variants of each twin mode can be obtained from a single twin variant by applying a series of 60° rotations around the **c**-axis. We utilize the calculated variants, twin misorientations $\mathbf{R}_{tw}$, and $\mathbf{M}_{tw}$to compute a consistent set of rotations and twin systems.

The effective Schmid factor was adopted from [36] and is defined in terms of the shear stress on the twin plane in the shearing direction normalized by the maximum shear

$$ESF = \frac{\sigma_{13}^{tw}}{2\tau_{\max}}. \tag{3}$$

The calculation of the maximum shear is taken from the eigen values of $\boldsymbol{\sigma}$ representing the maximum and minimum principle stress $(\sigma_1 - \sigma_3)/2$, such that the effective Schmid factor is in the range $-0.5 \leq ESF \leq 0.5$ regardless of sample stress state. Notably, (3) reduces to the MTEX function *SchmidFactor* for uniaxial stress states. To evaluate (3) for a parent grain and child grain, the active twin variant I is determined and the stress tensor is transformed to $\mathbf{C}_{tw}$ by

$$\boldsymbol{\sigma}_{parent}^{tw} = \mathbf{R}_{tw}^{I}\left(\mathbf{g}_{parent}\right)^{-1}\boldsymbol{\sigma}, \boldsymbol{\sigma}_{child}^{tw} = \mathbf{R}_{tw}^{I}(\mathbf{g}_{child})^{-1}\boldsymbol{\sigma} \tag{4}$$

The calculation of (4) can be applied to all possible twin variants, producing the relevant parent and child Schmid values used for studying twin variant selection [41,42,62]. The definition of *ESF will be utilized in Section 4 when reconstructing the twin family tree.*

Similar to prior investigations of high purity α-Ti (e.g. [16]), three twin modes were found and their parameters are summarized in Table 1. The twin misorientation tolerances utilized in this study β, $\beta_{relaxed}$, and ϕ, and their interpretation will be further discussed in the following section.

3.2. Cluster graph

The three main graphs used to enable twin classification and identification of the twin family tree are demonstrated in Fig. 4. The graph G_{frag} has nodes V_{frag} defined as grains fragments from EBSD reconstruction and edges E_{frag} that are between neighboring grain fragments sharing boundaries. Thus, the edges E_{frag} have properties between two grain fragments, and nodes have properties of grain fragments. The graph G_{clust} contains the same nodes as G_{frag}, *i. e.* $V_{clust} = V_{frag}$ and only the edges of G_{frag} that satisfy a twin relationship or some other merging criterion (discussed below) are kept such that E_{clust} is a subset of E_{frag} ($E_{clust} \subset E_{frag}$). The sets of continuously connected edges in E_{clust} form the grains of the undeformed microstructure which are referred to in this work as clusters. Note, that in the absence of edges, a cluster is an undeformed grain or grain fragment. The clusters in G_{clust} are interfaced with grain fragment datasets for plotting and calculating merge grain properties using the MTEX function *mergeGrains*. The final graph G_{fam} consists of grouping similar grain fragment orientations (families) in each cluster, where V_{fam} is defined as the families in a cluster and E_{fam} connects families that share a twin relationship. In the next section the reconstruction of families is discussed at length and G_{fam} is used to create a family tree for each cluster, but the concepts of families is also utilized in constructing G_{clust}.

In addition to the merging criterion currently published in literature that include twin relationships, low misorientation boundaries, geometrically necessary relationships such as fragments internal to another fragment, and user specified merging [36,37], we introduce reconstruction of G_{clust} based on non-local family relationships (i.e. no shared boundary twin relationship) and cluster geometry to address over segmentation in G_{clust}. The use of θ_{frag} between 1 and 2° during fragment reconstruction from EBSD points results in grain fragments produced by twinning further fragmenting by slip induced low angle boundaries. While one can argue for a larger θ_{frag} choice, the formation of low angle boundaries is a hallmark of highly deformed materials, and over segmentation is an important issue to address. The edges E_{frag} with misorientations that satisfy the $\beta_{frag} = 2°$ tolerance are not removed when constructing G_{clust}. As mentioned in Section 2, this approach was chosen so that edges can readily be removed if they represent an undesired relationship such as those produced by twin chaining across boundaries or a similarly orientated neighbor grain in the initial microstructure. Importantly, a minimum graph where vertices have at least one edge attached is sufficient for creating a cluster, and any missing boundary relationships do not affect the formation of G_{fam}. For this reason, automatic merging based on low misorientation or other criterion only use the minimum number of edges needed to complete

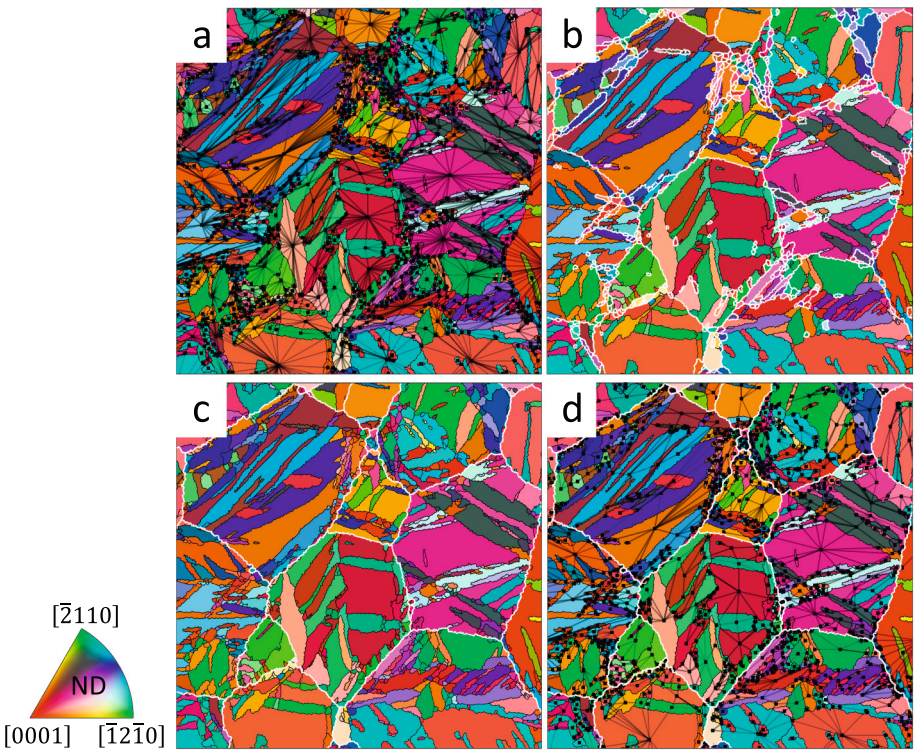

Fig. 5. Example of fragment reconstruction for ND loaded sample at a strain of 0.2. a) fragment graph connecting neighboring grain fragments, b) clusters (areas enclosed by white boundaries) after boundary based merging, c) clusters after geometric and family based merging, and d) clusters after geometric and family based merging with the cluster graph used to identify the clusters. Note that no cluster graph edge crosses a cluster boundary and that b, c, and d contain the same user modified edges, thereby geometric merging is isolated.

G_{clust}, thereby simplifying manual corrections by reducing the number of edges that need to be interacted with.

Twin modes have a separate merging β and classification tolerances $\beta_{relaxed}$ and ϕ as summarized in Table 1. The β is chosen to minimize the apparent user corrections needed in forming G_{clust}, while $\beta_{relaxed}$ is used to define the type of edge between two fragments for user interactions (i.e. adding edges, visualization, etc.). The ϕ is used during constructing G_{fam} in the next section. As pointed out in [37], the boundary based misorientation is expected to be the least accurate for twin identification. However, for these datasets with significant internal grain misorientation, the boundary based merging proved more sensitive at lower misorientation tolerances, resulting in less manual corrections when used in conjunction with additional merging criterion. Grain fragment boundary segments at junctions between more than two fragments (e.g. triple points) were removed from merging considerations since MTEX merging methodology using boundaries will cause a relationship between two grains to merge all grains associated with the boundary segment. The minimum length of grain boundary for a twin relationship to cause merging was implemented, but improvement by enforcing boundary length was negligible, and one boundary segment is used.

While increasing β greatly decreases the number of grains that are merged through secondary criterion such as cluster geometry, it also greatly increases the number of incorrectly merged boundaries. This appears to be especially prevalent given the orientation spread in families and the high number of unique twin families in the Ti datasets. Furthermore, the large number of twin lamella results in missing boundary relationships that require a non-local merging algorithm. Thus, we adopt an approach that utilizes a small β tolerance to limit incorrect boundaries and an iterative, cluster-based merging algorithm using the cluster size, shape, shared boundary ratio, and common families between clusters as a merging criterion.

Geometry criterion (cluster size, shape, shared boundary ratio) allows information about the initial microstructure to be leveraged, and the expected evolution of cluster geometry based on applied deformation can be used to identify a cluster that should not exist. Due to the large grain size and equiaxed initial grain shape of the Ti in this study, grains that are much smaller or have aspect ratios much higher than those in the initial microstructure, should be considered for merging with a neighboring cluster. For aspect ratio based merging, an aspect ratio of 3.5 and maximum cluster size of 9000 pixels was used (for reference the cluster in Fig. 7 is approximately 50,000 pixels). A maximum cluster size of 2000 pixels was adequate for identifying small clusters for merging.

For a cluster that has been flagged based on geometry, a criterion to merge with neighboring clusters is needed. Here we compare the mean family orientations (as calculated using the methodology described in the next section) with tolerances $\beta_{fam} = 12°$. The large tolerance is chosen to promote the merging of small clusters and overlapping twin domains (see Fig. 6). No merging is performed unless a common family is found, and when two neighboring clusters have the same number of common families, the merging is performed with the largest cluster. In addition to the geometry and family-based merging, most clusters that are internal to another cluster or partially internal should be merged. To this end, a shared boundary ratio was also defined, and when a cluster shares more than 70% of its boundary with another cluster, it was merged with that cluster.

The G_{frag}, clusters without geometric merging, clusters with geometric merging, and their relationship to the G_{clust} are demonstrated for select grains in Fig. 5. Geometric merging plays an important role in the reconstruction process. To gain some insight into the role of geometric merging, consider the EBSD of RD and ND at compressive strains of 0.2 and the β parameters in Table 1. Of the 38,076 nodes and 106,840 edges comprising the 685 clusters of the ND scan, 2675 clusters were merged by geometric considerations, 415 edges were removed and 3726 added manually. Of the 14,699 nodes and 37,727 edges comprising the 530 clusters of the RD scan, 2099 were merged by geometric considerations, 165 edges were removed and 142 added manually. Assuming the cluster merging could be done with a single manual operation, geometric and family-based merging reduced the amount of manual interaction from 6.4% to 3.9% for ND and from 6.4% to 0.8% for RD. The percentage of manual interaction at compressive strains of 0.05 were 0.9% for RD and

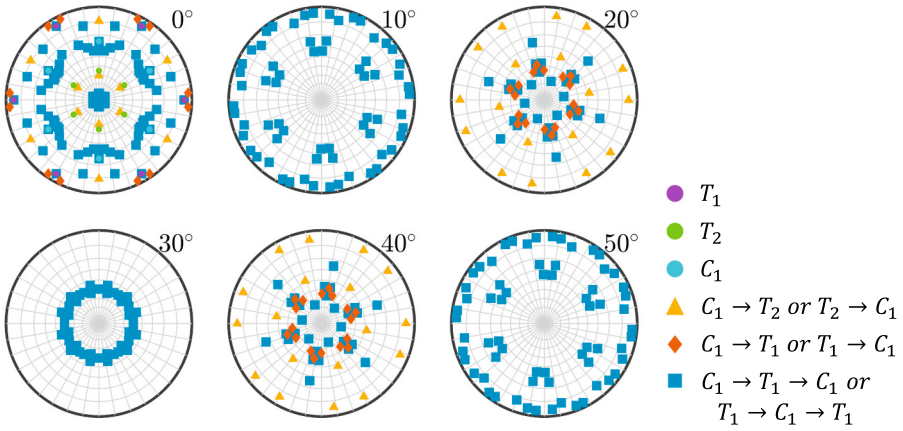

Fig. 6. Upper hemisphere {0001} pole figure sigma sections of prominent twins and higher order twinning sequences with respect to the unit cell. The sequences and twin types are the prominent relationships observed in the Ti dataset used in this study. The sigma section angle represents the rotation of the **c**-axis which in combination with crystal symmetry is representative of the twin orientations. For reference, the grid superimposed on the pole figures is 10°.

Table 2
A summary of the number of overlapping twin relationships that lead to circular relationships between families as a function of common twinning sequences in Ti and misorientation tolerance. The number of overlapping twins scales with the relaxation of the misorientation tolerance, and this should be a consideration during the choice of α if unique twin families are not to be merged.

Twinning sequence	Number of twin variants	Number circular relationships								
		Mis. Tolerance 5°			Mis. Tolerance 7.5°			Mis. Tolerance 10°		
		T_1	T_2	C_1	T_1	T_2	C_1	T_1	T_2	C_1
$T_1 \rightarrow C_1$ or $C_1 \rightarrow T_1$	36	–	–	–	12	–	–	12	–	–
$T_2 \rightarrow C_1$ or $C_1 \rightarrow T_2$	36	–	–	–	–	6	–	–	6	–
$C_1 \rightarrow T_1 \rightarrow C_1$	216	24	–	–	24	–	–	48	–	–
$T_1 \rightarrow C_1 \rightarrow T_1$	216	–	–	24	–	–	24	–	–	72
$C_1 \rightarrow T_1 \rightarrow C_1 \rightarrow T_1$ Or $T_1 \rightarrow C_1 \rightarrow T_1 \rightarrow C_1$	1296	12	–	–	12	–	132	12	12	264

1.2% for ND. Increasing β will shift these results away from boundary-based merging and the number of edges removed will go up. The optimal choice of β depends on the microstructure and is found through user estimation of the amount of manual interactions that will be needed to appropriately reconstruct G_{clust} and by weighing the ease of interacting with an over segmented microstructure versus under segmented microstructure.

3.3. Family graph

Fundamental to the approach of separating the grouping of fragments in G_{clust} and classification operations is the reconstruction of families which are groups of grain fragments of similar orientation in a cluster [36]. MTEX conveniently provides an agglomerative, hierarchical grouping function, *calcCluster*. The function takes a cluster and begins by merging the pair of orientations with the smallest misorientation. It then computes the mean of those orientations, assigns the orientations to a family group, and removes them from further consideration as the minimum misorientation. The misorientation of all other orientations in the cluster with respect to the mean orientation are updated, and the function iterates until no misorientation is smaller than a specified tolerance, α_{fam}. While this method is appropriate for grain fragments with minimal internal misorientation, disparate reorientation of family fragments at large strains and overlapping twin relationships are a major issue in the family reconstruction phase and later while assigning twin relationships between families.

Consider a family that was split in two due to an insufficiently large α_{fam}. During the classifications stage, one or both of the families may not have a twin relationship or both families may have the same type and twin variant. This can create multiple apparent roots for the family tree and result in higher order twinning since there can only be one root. If α_{fam} is increased too much in an attempt to group families with large misorientation, then depending on the twin types and higher order twinning, distinct families will be merged creating further classification issues. In Fig. 6 prominent twins and higher order twinning sequences are shown as calculated using (2) and the overlap of higher and lower order twin misorientations creating the same twin orientation within some tolerance are summarized in Table 2. Secondary and tertiary twins have clear overlap with primary twins, and likely no family reconstruction scheme will ensure appropriate groupings without considering twin geometric attributes and family tree reconstruction. The prevalence of overlapping twin families in the Ti datasets does not appear to be significant and a simple relaxation of α_{fam} is expected to produce satisfactory results. Careful manual investigation of clusters, such as that done in Fig. 7, revealed that α_{fam} greater than 4° will result in some higher order twins being merged with the root of lower order twins.

To address the sensitivity to the choice of the family grouping tolerance, we adopt a fragment based misorientation tolerance α_{frag} in combination with family reconstruction described above. First, *calcCluster* is used to group fragments into families. Then a fragment in Family A is merged into Family B if the Family A fragment shares an orientation with any Family B fragment less than the specified tolerance α_{frag}. The process is repeated until no more fragments are merged. This approach is like fragment reconstruction from EBSD data.

The result of the family clustering algorithm is demonstrated in Fig. 7 with an α_{fam} of 4° and α_{frag} of 0° and 2°. The EBSD IPF and the unique family fragment maps for a select grain are shown and several families were merged by using α_{frag} of 2°, reducing the total number of families

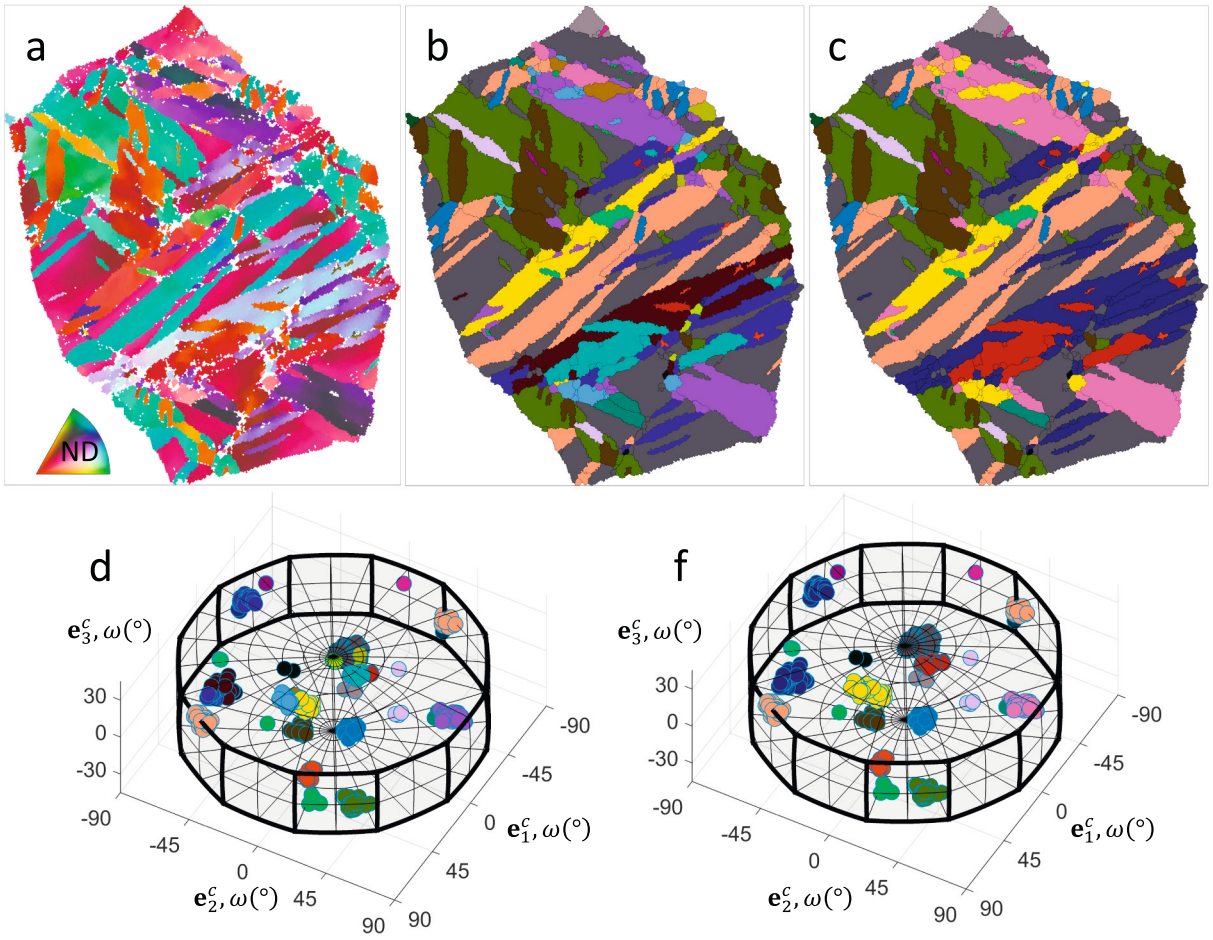

Fig. 7. Example of family merging algorithm applied with α_{fam}= 4° family tolerance (b,d) followed by α_{frag}= 2° fragment based merging (c,f) to a select grain with 200 μm equivalent diameter from the ND loaded sample and strain of 0.2. (a) is the as-cleaned EBSD IPF, (b, d) are the unique family grain plot and corresponding unique family clusters in angle-axis space without fragment merging, and (c, f) are the unique family grain plot and corresponding unique family clusters in angle-axis space with fragment merging. Note that the fundamental zone is used in plotting the angle-axis space, resulting in clusters continuing across the bounding surfaces of the space and that the directions $\mathbf{e}_i^c$are the directions of axes of the crystal frame.

from 30 to 22. The groupings of orientations are shown in the axis-angle space, giving an interpretation of disorientation (minimum misorientation), and the clustering algorithm captures the anisotropic cluster shapes and intuitive grouping of grain fragment based on the EBSD IPF. In the Fig. 7 there is at least one unmerged family and increasing either of the tolerances results in families being merged that clearly should not be merged. For the datasets here, increasing α_{frag} above 2° significant increases the incorrectly merged families, while increasing α_{fam} to 6° addresses prevalent classification issues in the family trees with minimal over-merging. Based on these observations, an α_{fam} of 6° and α_{frag} 2° is adopted in this work. For reference, the total number of families in Fig. 7 is further reduced to 17 with these tolerances.

The family graph G_{fam} is finally constructed for each cluster in G_{clust}. When determining twin relationships, the unweighted mean family orientation determined in *calcCluster* is replaced by the grain area weighted mean using the MTEX function *mean*. This approach biases the orientation importance in defining the twin relationships based on the assumption that more fragments will have shared boundaries with the larger fragments. The twin relationships are then calculated between the weighted mean orientations of families using the tolerance ϕ in Table 1. The choice of ϕ determines which family relationships are considered in the making of the family tree and a large tolerance (10° in this case) can be used so long as the family tree reconstruction process is able to isolate the relevant twin relationships.

3.4. Manual corrections of graphs

MTEX natively has the capability to interact with data through a programming interface. To facilitate quick interaction with the data, a command line wrapper to basic graph operations was developed. A list of cluster ids to edit are passed to the graph editor. For each cluster, commands such as removing and adding edges, testing relationships between fragments, and changing the plot visualization options are accessed through the MATLAB command window menus. To facilitate interacting with edges and nodes specifically, the MATLAB graph toolbox plotting capabilities are utilized to overlay node ids and edge ids on MTEX grain plots. This greatly simplifies interacting with data reconstruction in MTEX, and its utility is not limited to twin analysis.

The data structure introduced by graphs plays an important role in graph modifications. The G_{frag} and G_{clust} graphs have the same number of nodes, and the edges E_{clust} are a subset of edges E_{frag}. Therefore, all node and edge ids are stationary if the set of fragments reconstructed from EBSD is not changed. In this work, the edge ids for adding and removing edges are written to text files and read in at the construction of G_{clust}. The graph G_{fam} discussed in the previous section is only stationary if a cluster in G_{clust} is not modified. To address the computational overhead in large EBSD datasets such as those used in this study, the G_{fam} information is stored per cluster and modifications to the G_{clust} are tracked such that if a cluster does not change, quantities are not recomputed at the family level. Fig. 8 demonstrates the workflow including the manual graph

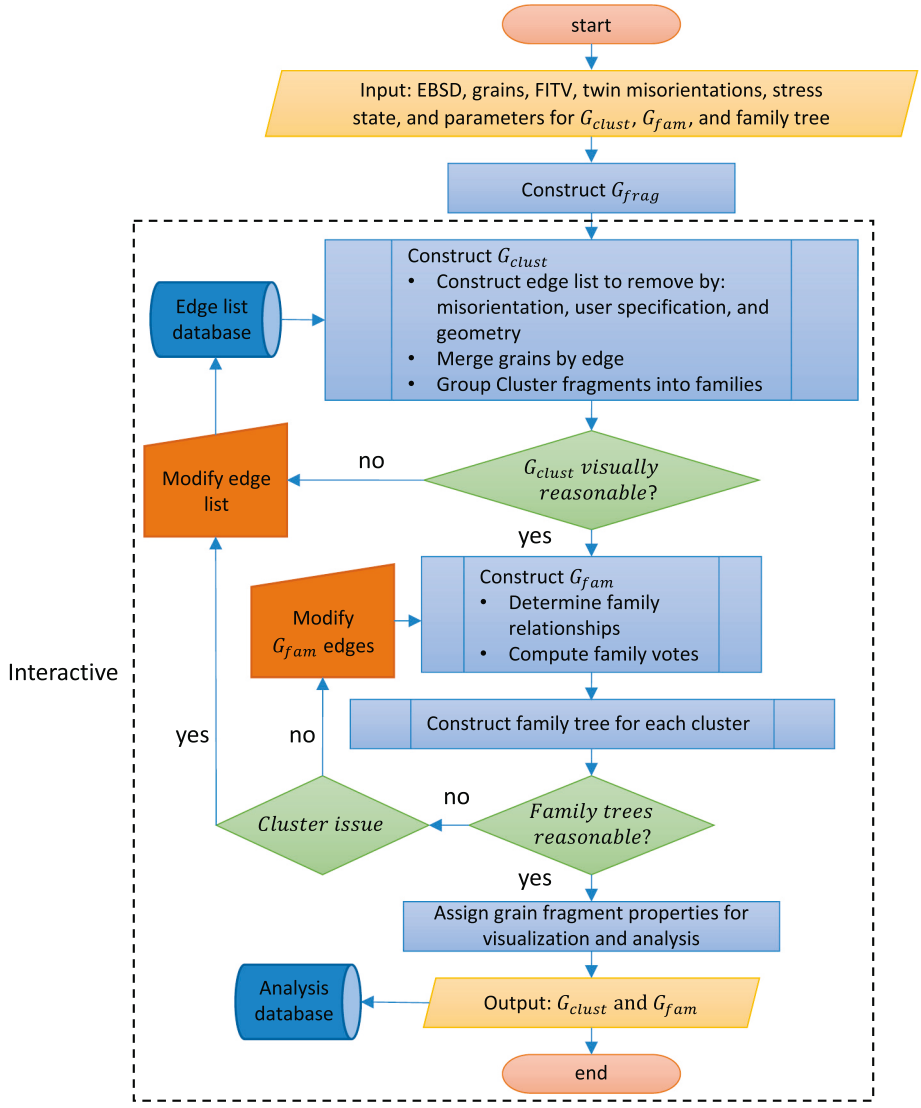

Fig. 8. The twin reconstruction workflow including the sequence of graph operations and incorporation of manual modifications as defined in Sections 3 and 4.

modifications. In this way manual interactions are stored and edits are incorporated in an efficient manner.

4. Family tree reconstruction

The family tree is a graph representing the hierarchy of twinning and contains the grain fragment properties of twin generation and twin type. The twin family tree is also equal to or a subset of G_{fam} and is only an output of graph operations performed on G_{fam}. The advantage of this approach versus using the G_{clust} directly in the computations becomes immediately apparent when data structure and manual interactions with the data are considered. As a result, there is no need to have a separate graph for the family tree; we continue to use G_{fam} in the computation of the family tree and store the results in G_{clust}.

To construct the family tree, the direction of the twin relationships must be known (i.e. for each edge in G_{fam}, one family is the parent and the other family a child). There are several strategies determining the direction of a twin relationship such as Schmid analysis, geometric considerations (e.g. boundary ratio and area ratio), and assumptions about the twinning process (e.g. twins cannot contain the same twin type). As a first step in determining the parent and child nodes for E_{fam}, the parent voting scheme of [36] is adopted. However, we do not adopt the main twinning rule of [36] (a family who has a relationship with two or more variants of the same twin type is the parent of those variants) because circular relationships with higher order twins satisfy the criterion (see Table 2 and Fig. 10). For families 1 and 2, the family with the highest relative vote

$$\begin{aligned} Vote_1 &= w_{FESF}(FESF_1 - FESF_2) + w_{FA}\left(\frac{FA_1 - FA_2}{FA_1 + FA_2}\right) + w_{FGBL}\left(\frac{FGBL_1 \cap FGBL_2}{FGBL_2} - \frac{FGBL_1 \cap FGBL_2}{FGBL_1}\right) \\ Vote_2 &= w_{FESF}(FESF_2 - FESF_1) + w_{FA}\left(\frac{FA_2 - FA_1}{FA_1 + FA_2}\right) + w_{FGBL}\left(\frac{FGBL_1 \cap FGBL_2}{FGBL_1} - \frac{FGBL_1 \cap FGBL_2}{FGBL_2}\right) \end{aligned} \quad (5)$$

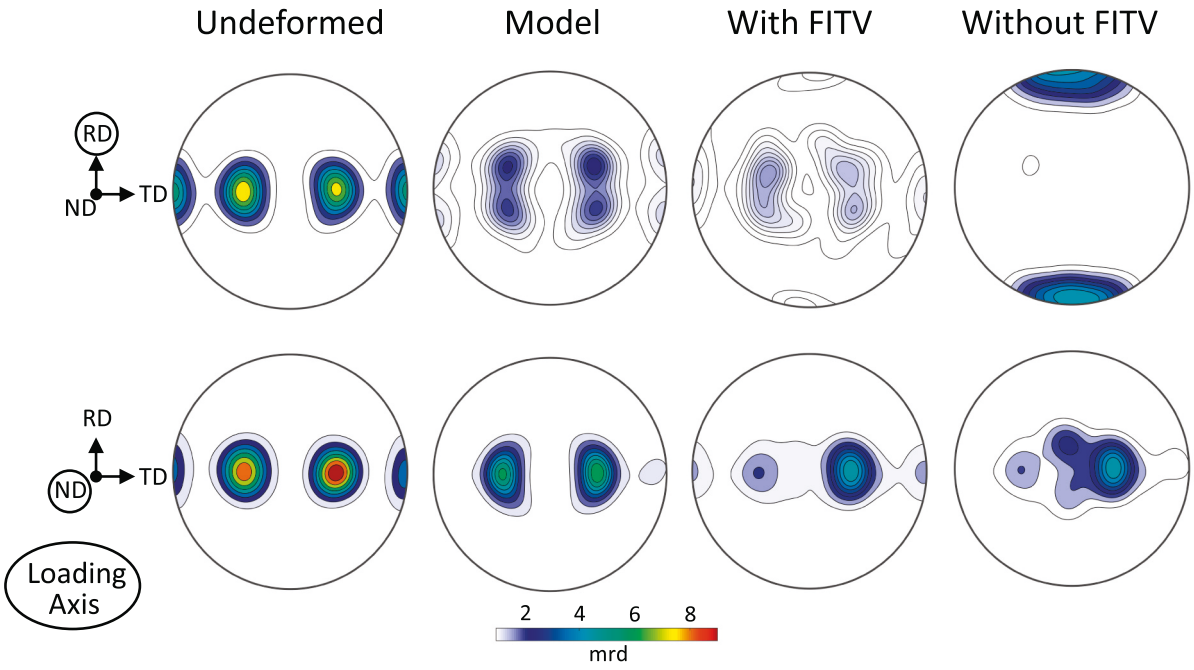

Fig. 9. {0001} pole figures comparing the undeformed, crystal plasticity model [64] and reconstructed root texture for RD and ND at compressive strains of 0.2. In the root textures, the orientations are calculated according to Eq. (9). In (column 1) the undeformed sample is shown for reference, (in column 2) the model, in (column 3) the family initial texture volume (*FITV*) is used in combination with node out-closeness (7) to identify the root family, and in (column 4) the root family is solely identified based on node out-closeness (6).

is the parent. Variables used in the voting scheme are as follows: *FESF* is the family effective Schmid factor as defined in (3), *FA* is the family area, *FGBL* is the family grain boundary length, and w_{FESF}, w_{FA}, and $w_{FGBL}$are weights. Note that each quantity is bounded between $-[w_{FESF}, w_{FA}, w_{FGBL}]$ and $[w_{FESF}, w_{FA}, w_{FGBL}]$, and that each term has a distinct meaning that can break down depending on the microstructure and twinning behavior. The *FESF* is a good indicator of the parent [41], but non-Schmid twinning behavior degrades performance. The *FA* is only a good identifier of the parent so long as the parent is larger than the twin. The FGBL is a good identifier of the parent when hierarchical twinning is dominant but is still sensitive to the twin fraction. Defining the edge direction from the parent to the child node, G_{fam} can be made into a directional graph. Directional graph operators and algorithms are a powerful class of tools and will be leveraged throughout the remainder of the section.

4.1. Determination of the root family

The tenant of some past twin analysis codes has been that the root of the family is the largest area [37,38] or simply the family that is not a child of any other family [36], i.e. the only family with all edges directed out of its node. However, in the α-Ti datasets at strains of 0.2, 33.8% of RD and 20.5% of ND clusters have more than one apparent root or no root at all due to circular relationships. Based on published approaches to constructing the family tree, those clusters would need to be solved manually. There are several reasons why having multiple apparent roots is possible: the cluster of fragments contains fragments from multiple grains in the initial microstructure, incorrect family grouping, missing root due to completely twinned grain, incorrect parent determination based on (5), and circular relationships which arise due to crystallography of twinning. Since family grouping is robust and the clustering of grains has been performed appropriately, it seems that most of the undetermined roots arise from (5) or due to a missing root. Addressing these issues manually would be time consuming and, for complex family graphs, unfeasible. In what follows, we describe a novel approach to determining the family tree that is robust against these issues.

First, let us consider the node centrality metric of out-closeness applied to the directional graph G_{fam} (per cluster) which for node i is defined as

$$c_i = \left(\frac{A_i}{N-1}\right)^2 \frac{1}{C_i}, \quad i = 1 \ldots N_{fam} \tag{6}$$

where A_i is the number of reachable nodes from node i, N is the number of nodes in G_{fam}, and C_i is the sum of distance from node i to all reachable nodes in G_{fam}. A reachable node from a given node i is defined based on the directional graph property of allowing graph traversal only along an edge's direction. Thus if a node has no outgoing edges, then (6) is zero; and if the distance for traversing each edge is 1, then the highest centrality score(s) is based solely on the number of nodes reached. An appropriate weighting scheme for edges that emulates the ideas presented in (5) is presented below in (8). Based on prior twin codes determining the root family as the family with only outgoing edges, the family with maximum out-closeness may be a reasonable way to determine the root family, thereby assimilating information from the entire graph.

The result of using the measure of node out-closeness (6) to determine the root family is shown in Fig. 9. Apparently, the measure does not reconstruct the initial texture for RD, and the root texture for ND is only partially reconstructed. Noticeably, the reconstructed textures do not appear to be consistent with classic streaking signatures of slip reorientation, and the material's deformation up to 0.2 strain is expected to be due largely to twinning based on crystal plasticity modeling of the Ti dataset [64]. The result is only a weak function of distance weights used $\{w_{FGBL}, w_{FESF}, w_{FA}, w_{gen}\} = \{1, 5, 0, 0\}$. The choice of weights was chosen to follow the twin family tree weights in the next section after observing that the weights improved results for ND over using weights of unity, and little was gained by using a custom set of weights. Based on these observations, the root is not being appropriately chosen using (6) alone.

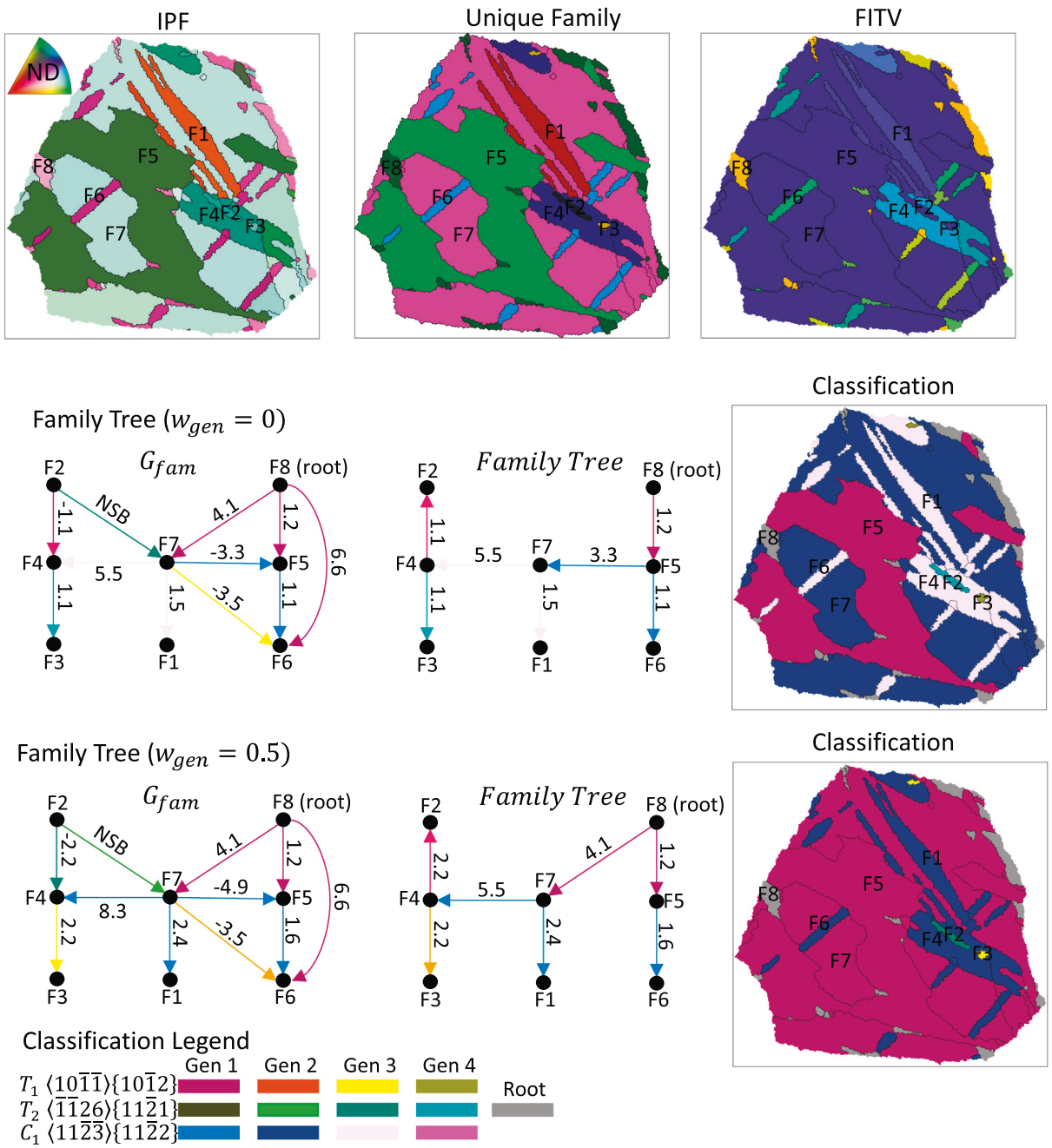

Fig. 10. A grain case study of higher ordering twinning for RD at a strain of 0.2 demonstrating how w_{gen} can affect the classification process. In the selected grain, a w_{gen} of 0 produces the twinning sequence $T_1 \rightarrow C_1 \rightarrow C_1 \rightarrow T_1/T_2$. For w_{gen} of 0.5, the twinning sequence becomes $T_1 \rightarrow C_1 \rightarrow T_1/T_2$. Both results are an intuitive interpretation of the twin family geometry given the IPF, Unique Family, and FITV grain maps. Labels preceded by "F" refer to the family number, NSB refers to no-share boundary which is criterion used to remove edges, and numbers on the edges correspond to the distance as computed by the spanning tree algorithm and (8). The negative distance denote that the direction of the distance computation is opposite the edge direction defined in (5) and the classification reflections the generation and twin type considered during the Prim algorithm.

To address the apparent deficiency of (6), we scale the centrality score by the family initial texture volume (*FITV*)

$$c_i = \left(\frac{A_i}{N-1}\right)^2 \frac{FITV_i}{C_i}, \quad i = 1 \ldots N_{fam} \tag{7}$$

To enable the calculation of *FITV*, the material frames of the EBSD scans were aligned using the apparent orthotropic sample symmetry and the *centerSpecimen* function in MTEX (as shown in Fig. 2). For a loading case and deformed G_{frag}, the volume fraction of each grain fragment orientation in the undeformed sample ODF was evaluated using the MTEX *volume* function with 10° radius. After family reconstruction, the *FITV* of a family is taken as the max FITV over the fragments in a family. The resulting root texture for samples strained to 0.2 are shown in Fig. 9. The metric in (7), which imposes the dual condition of describing the twin relationships and the initial ODF, appears to appropriately select the root family.

In this work, the main assumption of using the *FITV* is that reorientation by slip is minimal and the root family still exists. Both of these assumptions appear reasonable based on the results in Fig. 9–14. One way to address both issues for a more demanding dataset would be to reconstruct the parent phase at more frequent strain intervals, monitor the trends in area fractions, and utilizing the evolved FITV from prior

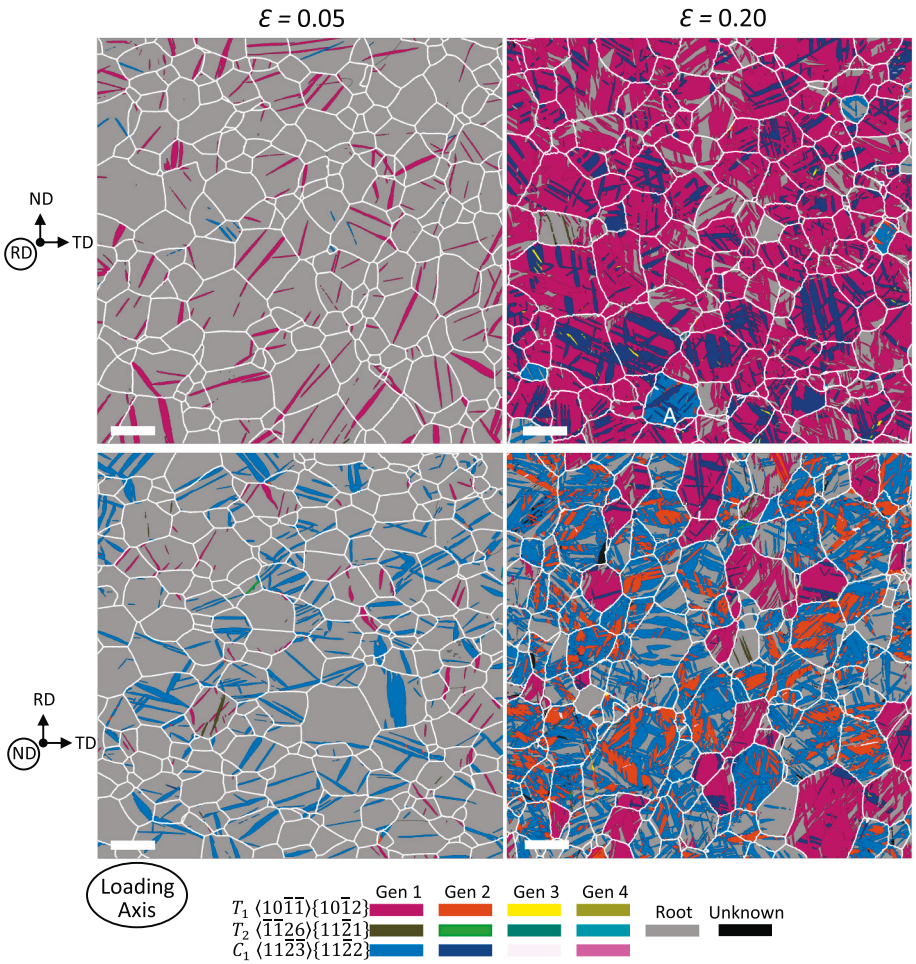

Fig. 11. Reconstructed grain cluster boundaries (white) overlaid on fragment twin classification map for RD and ND at strains of 0.05 and 0.2. Grain A in RD loading case is an example of a grain that has fully twinned. The scale bar is 200 μm.

strain intervals to inform the root selection and potentially detect a missing root based on a FITV threshold. Due to the strong initial texture, loading along RD that results in primary compression twinning is likely indicative of a missing root or twin relationship. In Fig. 11 there is one example of a cluster that is missing a root, but no attempt is made to automatically identify the missing root using texture or other means because missing roots do not appear to be prevalent based on the twinning sequences.

4.2. Determination of the family tree from the family graph

In graph theory, a common non-directional graph task is to find the set of edges that span all nodes while minimizing the sum cost of the edges, i.e. a minimum spanning tree (MST). A tree contains no circular relationships, and the cost to traverse an edge is taken here as L_E, where a lower traversal distance has a lower cost (see Fig. 10 for an example of reducing the family graph to the family MST). Utilizing an MST algorithm to determine the twin family tree will automatically address circular relationships and any fringe cases that arise. The main assumptions for building a valid family tree are: (1) that the grains are appropriately clustered/fragmented, (2) that there are no missing relationships between families, and (3) that the correct family-family relationships are those that best satisfy the geometric, loading, and twin nucleation assumptions. We note that in the absence of circular twin relationships and given the root family, the MST is identical to the graphs constructed in [36,37] and that most approaches to dealing with circular twin relationships and fringe cases (e.g. multi twin variant parent rules [36]) can be formulated in the context of an edge length minimization.

Many algorithms exist that allow that the minimum spanning graph to be constructed. An appropriate algorithm will allow the root of the tree to be specified and ensure that the tree emanates from the root. Here we adopt the methodology utilized in the so-called Prim algorithm [65] since the algorithm intuits the idea of a family begetting another family (i.e. hierarchical twinning). Starting from a specified root, the Prim type algorithm proceeds iteratively, by adding an edge that has the minimum traversal cost among candidate edges and does not create a circular relationship. Only edges which have one node in the spanning tree are considered, until no more nodes remain to be included in the spanning tree. Since the graph proceeds outward from the root, the directionality of relationships, i.e. from a node in the graph (parent) to a node not yet in the graph (child), can be calculated based on the following weighting procedures, wherein the traversal distance is taken as

$$L_E = \left(\frac{1 + w_{gen}\left(gen_{parent}\right)}{3\left(w_{FGBL} + w_{FESF} + w_{FAR}\right)} \begin{bmatrix} w_{FGBL}\dfrac{FGBL_{parent} \cap FGBL_{child}}{FGBL_{child}} + \dots \\ w_{FESF}\dfrac{FESF_{parent} + 0.5}{1} + \dots \\ w_{FA}\dfrac{FA_{parent}}{FA_{parent} + FA_{child}} \end{bmatrix} \right)^{-1}. \tag{8}$$

In this equation, *gen* is the generation of the parent node (zero if the root node), and the remaining terms are as defined as in (5). Each voting component can be removed by setting the corresponding weight to zero.

For the family tree determination, we restrict the valid twin

Table 3
Summary of EBSD scan size, the number of reconstructed grains N_{grain}, mean area weighted equivalent diameter based on reconstructed grains d_{eq}, the number grain fragment N_{frag}, and twin area fractions for T_1 and C_1. T_2 twins are not included in the table since their area fraction is less than 0.001 for the loading and texture conditions utilized in this study.

	Scan size (mm^2)	N_{grain}	d_{eq} (μm)	N_{frag}	T_1 area fractions		C_1 area fractions	
					1st gen.	2nd gen.	1st gen.	2nd gen.
RD-initial	13.279	1264	133.48	–	0	0	0	0
RD-5pct	3.129	402	141.86	1428	0.066	0	0.00	0
RD-20pct	3.499	442	150.20	12,709	0.643	0.002	0.013	0.171
ND-initial	11.328	1044	167.40	–	0	0	0	0
ND-5pct	3.398	483	129.90	2695	0.010	0	0.100	0
ND-20pct	3.542	572	152.04	33,810	0.177	0.097	0.326	0.023

relationships to those between families that share boundaries, unless the criterion removes a family completely in which case all twin relationships are used for that family. The weights $\{w_{FGBL}, w_{FESF}, w_{FA}, w_{gen}\} = \{1, 5, 0, 0.5\}$ are adopted due the large area fraction of twins and to promote in the absence of a clear Schmid based behavior the family grain boundary length which should work well for hierarchical twinning. The generation weight was chosen to promote the addition of lower order twins during the Prim type spanning tree algorithm and can be thought of as a relaxed implementation of level graph sideward pruning. This helps ensure that all edges describing higher order twinning are being considered in G_{fam}, and provides the option to test the sensitivity of reconstruction results to the algorithm. The generation weight of 0.5 was chosen here such that highly favorable, higher order twin relationships can still be added to the family tree before lower order twin relationships that are not favorable.

It is important to acknowledge that while the relationships are not explicitly enforced, the weighting parameters and methodology bias the results towards hierarchical twinning. To help demonstrate the importance of the point, a grain was identified from Fig. 11 for RD loaded to 0.2 strain in which the twin hierarchy changing based on w_{gen}. A w_{gen} of 0 produces the twinning sequence $T_1 \rightarrow C_1 \rightarrow C_1 \rightarrow T_1/T_2$ suggesting fourth order twinning. For w_{gen} of 0.5 the twinning sequence becomes $T_1 \rightarrow C_1 \rightarrow T_1/T_2$ which reveals a twinning sequence $T_1 \rightarrow C_1 \rightarrow T_2$ that has not been observed in α-Ti. Inspection of the traversal distance calculated by the MST algorithm, the shared boundary, and geometric nesting reveal either result could be reasonable.

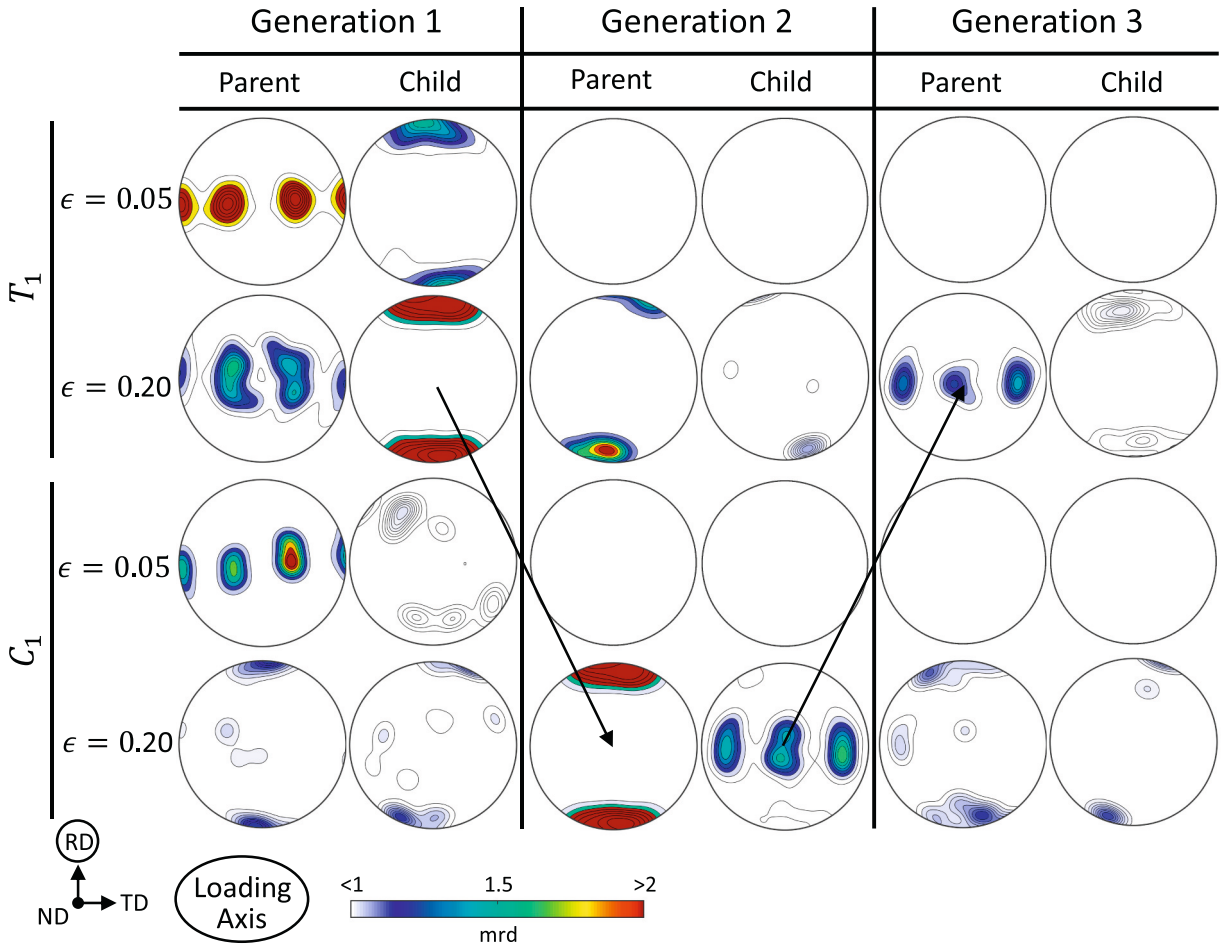

Fig. 12. Hierarchical twinning with the sequence $T_1 \rightarrow C_1 \rightarrow T_1$ is shown in {0001} pole figures using the twin classification of parent-child relationships for RD loaded at two strain levels. For interpretation of the intensity plotted intensities, see (9).

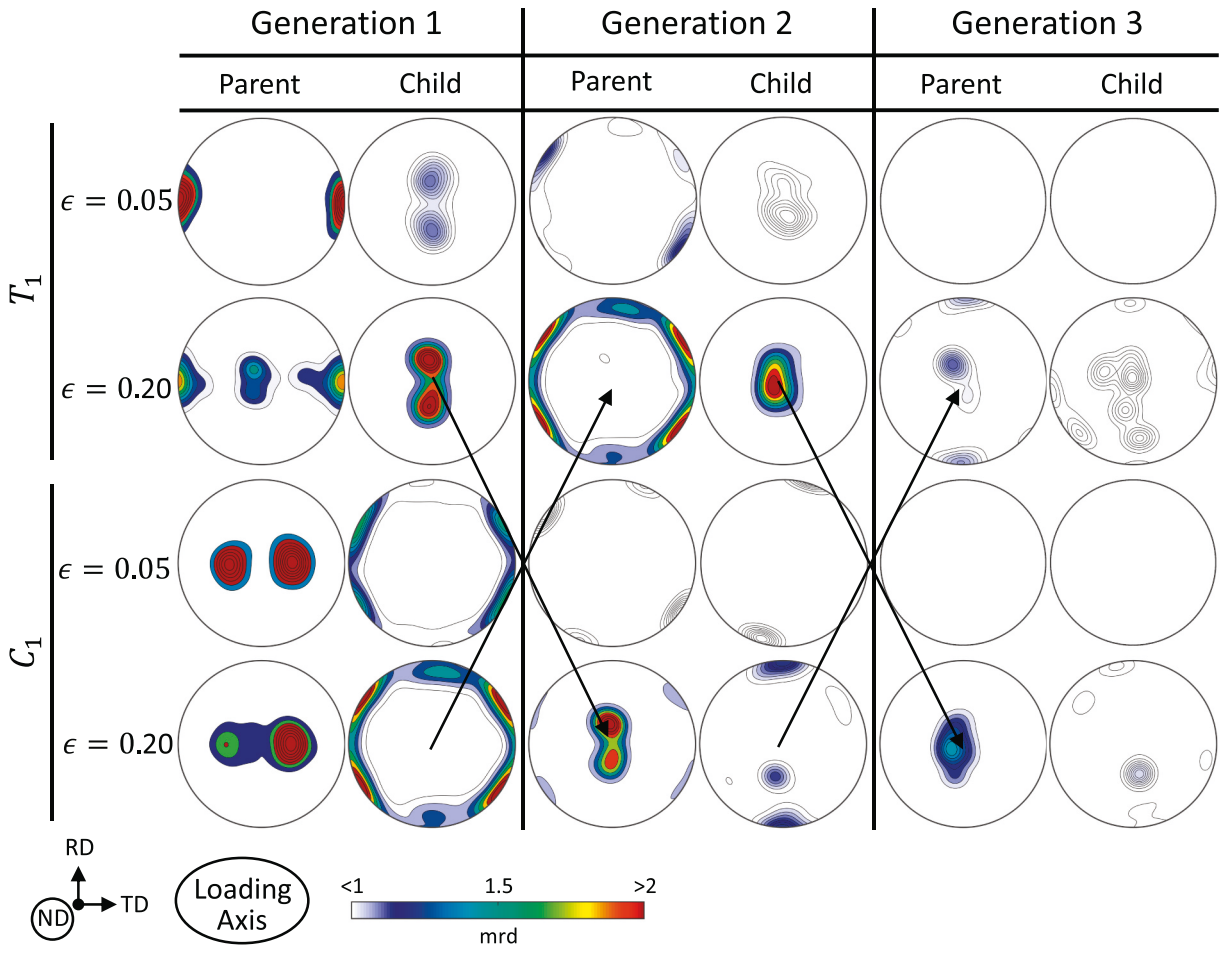

Fig. 13. Hierarchical twinning with the sequence $T_1 \rightarrow C_1 \rightarrow T_1$ and $C_1 \rightarrow T_1 \rightarrow C_1$ is shown in {0001} pole figures using the twin classification of parent-child relationships for ND loaded at two strain levels. For interpretation of the intensity plotted intensities, see (9).

5. Results and discussion of reconstructed Ti dataset

The reconstructed cluster boundaries are shown in Fig. 11, and the corresponding mean grain size is summarized in Table 3. As expected, the grain size increases in the plane of compression except for ND initial and ND 0.05 strain. This appears to be a result of grain size variation between samples since the reconstruction at strains of 0.05 is visually correct. In general, similar morphological characteristics are recovered for 0.05 and 0.2 clusters when compared with the initial grain maps in Fig. 3, giving some confidence that the grouping of fragments is reasonable. Here a combined automatic and manually reconstruction was performed as discussed in section 3.2. The results of the twin classification map were used to highlight and inform the clustering process.

No edits to the family trees were performed on datasets at a strain of 0.05 while 9 ND and 16 RD clusters in datasets at strain of 0.2 had family trees edited. The main issue observed was a breakdown of (7) due to twins having a large FITV value. The twin area fraction as a function of generation is also reported in Table 3 and visualized in Fig. 11. We see a continuation of twinning trends at 0.05 strain in the 0.2 strain materials. Remarkably, secondary twins occur in large area fractions reaching 17.1% for secondary compression twinning for loading in RD and 9.7% for secondary tensile twinning in ND. Tertiary twinning that satisfies clear hierarchical geometries are observed but do not have significant volume contributions. Quaternary twins are also observed, though these do not satisfy clear hierarchical geometries, suggesting that they are reconstruction artifacts such as in Fig. 10. Should the secondary twinning in the RD case increase significantly with continued straining, it is possible that tertiary twinning could become significant in large grained α-Ti.

Using the novel procedures developed here, Fig. 11 demonstrates a successful clustering of fragments and the twin classification map follows the expected twinning trends. However, having a more quantitative insight into parent-child twin paradigm is desirable. To visualize the texture reorientation characteristics between parent and twin grains as a function of twin generation, orientation distribution functions were constructed for the common types and generations of twins. In MTEX, ODFs can be formed by a summation of single component ODFs. Furthermore, ODFs can be diluted by adding a uniform ODF background as in

$$ODF_{gen,type} = \frac{\sum A_{gen,type}}{\sum A} componentODF\left(g_{gen,type}, A_{gen,type}\right) + \left(1 - \frac{\sum A_{gen,type}}{\sum A}\right) uniformODF \quad (9)$$

where the generation and type is the classification of fragments as visualized in Fig. 11. The grain fragment area is A and the mean grain fragment orientations is g. The resulting {0001} pole figures for the parent and twin for each type, generation, and strain level are presented for RD in Fig. 12 and for ND in Fig. 13. These figures represent the twin and parent texture strength in the ODF $componentODF(g,A)$. The family tree reconstruction captures hierarchical twinning up through tertiary twinning, following a $T_1 \rightarrow C_1 \rightarrow T_1$ sequence for RD and a combination of $T_1 \rightarrow C_1 \rightarrow T_1$ and $C_1 \rightarrow T_1 \rightarrow C_1$ in ND. Figs. 12 and 13 demonstrate

that on a statistical level the family classification proposed in the work reproduces the expected hierarchical twinning signatures.

6. Summary and conclusions

A general twin code implementation is presented leveraging the MATLAB graph toolbox and MTEX toolbox. Novel algorithms for grain fragment grouping and segmentation are presented and their parameters justified. In particular, we developed novel non-local clustering methods and adapt family determination to include anisotropic misorientation domains. We show that the root determination rule based solely on parent-child determination is insufficient for highly twinned microstructures, and we propose a novel metric combining texture and graph centrality to identify the root. A general procedure for twin family tree determination is presented that automatically addresses complex twin relationships that arise in heavily twinned microstructures and its utility is demonstrated on a demanding α-Ti dataset. The results are a compelling example of the utility of the code for studying twinning in metals. The approach reveals that α-Ti will continue to at least third generation twinning and that higher order twins occur independent of the starting twinning sequence (i.e. $T_1 \rightarrow C_1$ versus $C_1 \rightarrow T_1$).

Data availability

The raw data and archived git repository associated with this work can be found at https://github.com/djm87/Twin-Analysis.

Declaration of Competing Interest

The authors declare that they have no known competing financial interests or personal relationships that could have appeared to influence the work reported in this paper.

Acknowledgements

This research was sponsored by the U.S. National Science Foundation and was accomplished under the CAREER grant no. CMMI-1650641. DJS gratefully acknowledges partial support through the University of New Hampshire Dissertation Year Fellowship and the Seaborg Institute under a post-doctoral fellowship through the Los Alamos National Laboratory LDRD program. RJM acknowledges support through the Office of Basic Energy Sciences, Project FWP 06SCPE401, under US DOE contract no. W-7405-ENG-36.

References

[1] J.W. Christian, S. Mahajan, Deformation twinning, Prog. Mater. Sci. 39 (1995) 1–157.
[2] M. Ardeljan, I.J. Beyerlein, M. Knezevic, Effect of dislocation density-twin interactions on twin growth in AZ31 as revealed by explicit crystal plasticity finite element modeling, Int. J. Plast. 99 (2017) 81–101.
[3] M. Knezevic, A. Levinson, R. Harris, R.K. Mishra, R.D. Doherty, S.R. Kalidindi, Deformation twinning in AZ31: influence on strain hardening and texture evolution, Acta Mater. 58 (2010) 6230–6242.
[4] A.S. Khan, A. Pandey, T. Gnäupel-Herold, R.K. Mishra, Mechanical response and texture evolution of AZ31 alloy at large strains for different strain rates and temperatures, Int. J. Plast. 27 (2011) 688–706.
[5] G.-S. Song, S.-H. Zhang, L. Zheng, L. Ruan, Twinning, grain orientation and texture variation of AZ31 mg alloy during compression by EBSD tracing, J. Alloys Compd. 509 (2011) 6481–6488.
[6] J.R. Luo, A. Godfrey, W. Liu, Q. Liu, Twinning behavior of a strongly basal textured AZ31 mg alloy during warm rolling, Acta Mater. 60 (2012) 1986–1998.
[7] X.Q. Guo, A. Chapuis, P.D. Wu, S.R. Agnew, On twinning and anisotropy in rolled mg alloy AZ31 under uniaxial compression, Int. J. Solids Struct. 64-65 (2015) 42–50.
[8] M. Jahedi, B.A. McWilliams, P. Moy, M. Knezevic, Deformation twinning in rolled WE43-T5 rare earth magnesium alloy: influence on strain hardening and texture evolution, Acta Mater. 131 (2017) 221–232.
[9] B.C. Wonsiewicz, W.A. Backofen, Plasticity of magnesium crystals, Trans. Metall. Soc. AIME 239 (1967).
[10] H. Yoshinaga, T. Obara, S. Morozumi, Twinning deformation in magnesium compressed along the C-axis, Mater. Sci. Eng. 12 (1973) 255–264.
[11] R. Reed-Hill, W. Robertson, Additional modes of deformation twinning in magnesium, Acta Metall. 5 (1957) 717–727.
[12] D. Ando, J. Koike, Y. Sutou, The role of deformation twinning in the fracture behavior and mechanism of basal textured magnesium alloys, Mater. Sci. Eng. A 600 (2014) 145–152.
[13] M.R. Barnett, Twinning and the ductility of magnesium alloys: Part II. "Contraction" twins, Mater. Sci. Eng. A 464 (2007) 8–16.
[14] P. Cizek, M.R. Barnett, Characteristics of the contraction twins formed close to the fracture surface in mg-3Al-1Zn alloy deformed in tension, Scr. Mater. 59 (2008) 959–962.
[15] S. Ghorbanpour, B.A. McWilliams, M. Knezevic, Low-cycle fatigue behavior of rolled WE43-T5 magnesium alloy, Fatigue Fract. Eng. Mater. Struct. 42 (2019) 1357–1372.
[16] V. Livescu, I.J. Beyerlein, C.A. Bronkhorst, O.F. Dippo, B.G. Ndefru, L. Capolungo, H.M. Mourad, Microstructure insensitive twinning: a statistical analysis of incipient twins in high-purity titanium, Materialia 6 (2019) 100303.
[17] W.G. Feather, S. Ghorbanpour, D.J. Savage, M. Ardeljan, M. Jahedi, B. A. McWilliams, N. Gupta, C. Xiang, S.C. Vogel, M. Knezevic, Mechanical response, twinning, and texture evolution of WE43 magnesium-rare earth alloy as a function of strain rate: experiments and multi-level crystal plasticity modeling, Int. J. Plast. 120 (2019) 180–204.
[18] M. Knezevic, M. Zecevic, I.J. Beyerlein, J.F. Bingert, R.J. McCabe, Strain rate and temperature effects on the selection of primary and secondary slip and twinning systems in HCP Zr, Acta Mater. 88 (2015) 55–73.
[19] X. Wu, S.R. Kalidindi, C. Necker, A.A. Salem, Prediction of crystallographic texture evolution and anisotropic stress-strain curves during large plastic strains in high purity α-titanium using a Taylor-type crystal plasticity model, Acta Mater. 55 (2007) 423–432.
[20] R.A. Lebensohn, C.N. Tomé, A self-consistent anisotropic approach for the simulation of plastic deformation and texture development of polycrystals: application to zirconium alloys, Acta Metall. Mater. 41 (1993) 2611–2624.
[21] M. Wronski, M. Arul Kumar, L. Capolungo, R.J. McCabe, K. Wierzbanowski, C. N. Tomé, Deformation behavior of CP-titanium: experiment and crystal plasticity modeling, Mater. Sci. Eng. A 724 (2018) 289–297.
[22] G. Proust, C.N. Tomé, G.C. Kaschner, Modeling texture, twinning and hardening evolution during deformation of hexagonal materials, Acta Mater. 55 (2007) 2137–2148.
[23] M. Knezevic, M.R. Daymond, I.J. Beyerlein, Modeling discrete twin lamellae in a microstructural framework, Scr. Mater. 121 (2016) 84–88.
[24] M. Zecevic, I.J. Beyerlein, M. Knezevic, Activity of pyramidal I and II <c+a> slip in mg alloys as revealed by texture development, J. Mech. Phys. Solids 111 (2018) 290–307.
[25] S.R. Kalidindi, H.K. Duvvuru, M. Knezevic, Spectral calibration of crystal plasticity models, Acta Mater. 54 (2006) 1795–1804.
[26] J. Wang, M. Zecevic, M. Knezevic, I.J. Beyerlein, Polycrystal plasticity modeling for load reversals in commercially pure titanium, Int. J. Plast. 125 (2020) 294–313.
[27] M. Knezevic, I.J. Beyerlein, D.W. Brown, T.A. Sisneros, C.N. Tomé, A polycrystal plasticity model for predicting mechanical response and texture evolution during strain-path changes: application to beryllium, Int. J. Plast. 49 (2013) 185–198.
[28] M. Knezevic, L. Capolungo, C.N. Tomé, R.A. Lebensohn, D.J. Alexander, B. Mihaila, R.J. McCabe, Anisotropic stress-strain response and microstructure evolution of textured α-uranium, Acta Mater. 60 (2012) 702–715.
[29] M. Knezevic, J. Crapps, I.J. Beyerlein, D.R. Coughlin, K.D. Clarke, R.J. McCabe, Anisotropic modeling of structural components using embedded crystal plasticity constructive laws within finite elements, Int. J. Mech. Sci. 105 (2016) 227–238.
[30] M. Knezevic, R.J. McCabe, R.A. Lebensohn, C.N. Tomé, C. Liu, M.L. Lovato, B. Mihaila, Integration of self-consistent polycrystal plasticity with dislocation density based hardening laws within an implicit finite element framework: application to low-symmetry metals, J. Mech. Phys. Solids 61 (2013) 2034–2046.
[31] M. Knezevic, R.J. McCabe, C.N. Tomé, R.A. Lebensohn, S.R. Chen, C.M. Cady, G. T. Gray Iii, B. Mihaila, Modeling mechanical response and texture evolution of α-uranium as a function of strain rate and temperature using polycrystal plasticity, Int. J. Plast. 43 (2013) 70–84.
[32] M. Zecevic, M. Knezevic, I.J. Beyerlein, R.J. McCabe, Origin of texture development in orthorhombic uranium, Mater. Sci. Eng. A 665 (2016) 108–124.
[33] M. Zecevic, M. Knezevic, I.J. Beyerlein, R.J. McCabe, Texture formation in orthorhombic alpha-uranium under simple compression and rolling to high strains, J. Nucl. Mater. 473 (2016) 143–156.
[34] S.R. Niezgoda, A.K. Kanjarla, I.J. Beyerlein, C.N. Tomé, Stochastic modeling of twin nucleation in polycrystals: an application in hexagonal close-packed metals, Int. J. Plast. 56 (2014) 119–138.
[35] M. Ardeljan, M. Knezevic, Explicit modeling of double twinning in AZ31 using crystal plasticity finite elements for predicting the mechanical fields for twin variant selection and fracture analyses, Acta Mater. 157 (2018) 339–354.
[36] P.E. Marshall, G. Proust, J.T. Rogers, R.J. McCabe, Automatic twin statistics from electron backscattered diffraction data, J. Microsc. 238 (2010) 218–229.
[37] C. Pradalier, P.-A. Juan, R.J. McCabe, L. Capolungo, A graph theory-based automated twin recognition technique for Electron backscatter diffraction analysis, Integr. Mater. Manuf. Innov. 7 (2018) 12–27.
[38] S.I. Wright, J.F. Bingert, T.A. Mason, R.J. Larson, Advanced Characterization of Twins Using Automated Electron Backscatter Diffraction, Los Alamos National Laboratory, 2002.
[39] B.L. Henrie, T.A. Mason, J.F. Bingert, Automated Twin Identification Technique for Use with Electron Backscatter Diffraction, Materials Science Forum, Trans Tech Publ, 2005, pp. 191–196.

[40] S. Ghorbanpour, B.A. McWilliams, M. Knezevic, Effect of hot working and aging heat treatments on monotonic, cyclic, and fatigue behavior of WE43 magnesium alloy, Mater. Sci. Eng. A 747 (2019) 27–41.
[41] L. Capolungo, P.E. Marshall, R.J. McCabe, I.J. Beyerlein, C.N. Tomé, Nucleation and growth of twins in Zr: a statistical study, Acta Mater. 57 (2009) 6047–6056.
[42] É. Martin, L. Capolungo, L. Jiang, J.J. Jonas, Variant selection during secondary twinning in mg–3%Al, Acta Mater. 58 (2010) 3970–3983.
[43] X. Fang, K. Zhang, H. Guo, W. Wang, B. Zhou, Twin-induced grain boundary engineering in 304 stainless steel, Mater. Sci. Eng. A 487 (2008) 7–13.
[44] Z. Zeng, S. Jonsson, H.J. Roven, The effects of deformation conditions on microstructure and texture of commercially pure Ti, Acta Mater. 57 (2009) 5822–5833.
[45] B.M. Morrow, R.J. McCabe, E.K. Cerreta, C.N. Tomé, Variability in EBSD statistics for textured zirconium, Mater. Sci. Eng. A 574 (2013) 157–162.
[46] M. Knezevic, S.R. Kalidindi, Fast computation of first-order elastic-plastic closures for polycrystalline cubic-orthorhombic microstructures, Comput. Mater. Sci. 39 (2007) 643–648.
[47] I. Chelladurai, D. Adams, D.T. Fullwood, M.P. Miles, S. Niezgoda, I.J. Beyerlein, M. Knezevic, Modeling of trans-grain twin transmission in AZ31 via a neighborhood-based viscoplastic self-consistent model, Int. J. Plast. 117 (2019) 21–32.
[48] E. Vasilev, M. Zecevic, R.J. McCabe, M. Knezevic, Experimental verification of a crystal plasticity-based simulation framework for predicting microstructure and geometric shape changes: application to bending and Taylor impact testing of Zr, Int. J. Impact Eng. 144 (2020) 103655.
[49] M. Zecevic, I.J. Beyerlein, R.J. McCabe, B.A. McWilliams, M. Knezevic, Transitioning rate sensitivities across multiple length scales: microstructure-property relationships in the Taylor cylinder impact test on zirconium, Int. J. Plast. 84 (2016) 138–159.
[50] M. Jahedi, B.A. McWilliams, M. Knezevic, Deformation and fracture mechanisms in WE43 magnesium-rare earth alloy fabricated by direct-chill casting and rolling, Mater. Sci. Eng. A 726 (2018) 194–207.
[51] M. Knezevic, R.A. Lebensohn, O. Cazacu, B. Revil-Baudard, G. Proust, S.C. Vogel, M.E. Nixon, Modeling bending of α-titanium with embedded polycrystal plasticity in implicit finite elements, Mater. Sci. Eng. A 564 (2013) 116–126.
[52] W. Tirry, M. Nixon, O. Cazacu, F. Coghe, L. Rabet, The importance of secondary and ternary twinning in compressed Ti, Scr. Mater. 64 (2011) 840–843.
[53] J.J. Bhattacharyya, F. Wang, P.D. Wu, W.R. Whittington, H. El Kadiri, S.R. Agnew, Demonstration of alloying, thermal activation, and latent hardening effects on quasi-static and dynamic polycrystal plasticity of mg alloy, WE43-T5, plate, Int. J. Plast. 81 (2016) 123–151.
[54] R.J. McCabe, G. Proust, E.K. Cerreta, A. Misra, Quantitative analysis of deformation twinning in zirconium, Int. J. Plast. 25 (2009) 454–472.
[55] F. Bachmann, R. Hielscher, H. Schaeben, Grain detection from 2d and 3d EBSD data—specification of the MTEX algorithm, Ultramicroscopy 111 (2011) 1720–1733.
[56] M. Zecevic, M. Knezevic, I.J. Beyerlein, C.N. Tomé, An elasto-plastic self-consistent model with hardening based on dislocation density, twinning and de-twinning: application to strain path changes in HCP metals, Mater. Sci. Eng. A 638 (2015) 262–274.
[57] M. Zecevic, I.J. Beyerlein, M. Knezevic, Coupling elasto-plastic self-consistent crystal plasticity and implicit finite elements: applications to compression, cyclic tension-compression, and bending to large strains, Int. J. Plast. 93 (2017) 187–211.
[58] N.C. Ferreri, D.J. Savage, M. Knezevic, Non-acid, alcohol-based electropolishing enables high-quality electron backscatter diffraction characterization of titanium and its alloys: application to pure Ti and Ti-6Al-4V, Mater. Charact. 166 (2020) 110406.
[59] U.F. Kocks, C.N. Tomé, H.-R. Wenk, Texture and Anisotropy: Preferred Orientations in Polycrystals and their Effect on Materials Properties, Cambridge university press, 1998.
[60] R.W. Cahn, Twinned crystals, Adv. Phys. 3 (1954) 363–445.
[61] M. Lentz, M. Risse, N. Schaefer, W. Reimers, I.J. Beyerlein, Strength and ductility with {1011} - {1012} double twinning in a magnesium alloy, Nat. Commun. 7 (2016) 11068.
[62] S.R. Niezgoda, A.K. Kanjarla, I.J. Beyerlein, C.N. Tomé, Stochastic modeling of twin nucleation in polycrystals: an application in hexagonal close-packed metals, Int. J. Plast. 56 (2014) 119–138.
[63] R.M. Wood, The lattice constants of high purity alpha titanium, Proc. Phys. Soc. 80 (1962) 783–786.
[64] D.J. Savage, Z. Feng, M. Knezevic, Identification of Crystal Plasticity Model Parameters by Multi-Objective Optimization Integrating Microstructural Evolution and Mechanical Data, 2020.
[65] R.C. Prim, Shortest connection networks and some generalizations, Bell Syst. Tech. J. 36 (1957) 1389–1401.